Pulse-delay effects in the angular distribution of near-threshold EUV + IR two-photon ionization of Ne

S. Mondal,[1] H. Fukuzawa,[1,2] K. Motomura,[1] T. Tachibana,[1] K. Nagaya,[2,3] T. Sakai,[3] K. Matsunami,[3] S. Yase,[3] M. Yao,[3] S. Wada,[2,4] H. Hayashita,[4] N. Saito,[2,5] C. Callegari,[6] K. C. Prince,[6,7] C. Miron,[8] M. Nagasono,[2] T. Togashi,[9] M. Yabashi,[2] K. L. Ishikawa,[10] A. K. Kazansky,[11,12,13] N. M. Kabachnik,[1,12,14] and K. Ueda[1,2]

[1]*Institute of Multidisciplinary Research for Advanced Materials, Tohoku University, Sendai 980-8577, Japan*

[2]*RIKEN SPring-8 Center, Kouto 1-1-1, Sayo, Hyogo 679-5148, Japan*

[3]*Graduate School of Science, Kyoto University, Kyoto 606-8502, Japan*

[4]*Graduate School of Science, Hiroshima University, Higashi-Hiroshima 739-8526, Japan*

[5]*National Institute of Advanced Industrial Science and Technology, NMIJ, Tsukuba 305-8568, Japan*

[6]*Elettra-Sincrotrone Trieste, 34149 Basovizza, Trieste, Italy*

[7]*eChemistry Laboratory, Faculty of Life and Social Sciences, Swinburne University of Technology, Melbourne, Victoria 3122, Australia*

[8]*Synchrotron SOLEIL, L'Orme des Merisiers, Saint-Aubin, BP 48, FR-91192 Gif-sur Yvette Cedex, France*

[9]*Japan Synchrotron Radiation Research Institute, Kouto 1-1-1, Sayo, Hyogo 679-5198, Japan*

[10]*Photon Science Center, Graduate School of Engineering, University of Tokyo, Tokyo 113-8656, Japan*

[11]*Departamento de Fisica de Materiales, UPV/EHU, E-20018 San Sebastian/Donostia, Spain*

[12]*Donostia International Physics Center, E-20018 San Sebastian/Donostia, Spain*

[13]*IKERBASQUE, Basque Foundation for Science, E-48011 Bilbao, Spain*

[14]*Skobeltsyn Institute of Nuclear Physics, Lomonosov Moscow State University, Moscow 119991, Russia*

(Received 17 August 2013; published 21 January 2014)

Photoelectron angular distributions (PADs) from two-photon near-threshold ionization of Ne atoms by the combined action of femtosecond pulses from an extreme ultraviolet (EUV) free-electron laser and infrared (IR) laser have been studied experimentally and theoretically. Solutions of the time-dependent Schrödinger equation indicate that the PADs strongly depend on the time delay between EUV and IR pulses. The experimental results obtained for two extreme cases of completely overlapping and nonoverlapping pulses fully confirm the prediction, illustrating that the measurements of the time-delay dependence of the PAD provide a tool for investigating the fundamental problem of the relative importance of the resonant and nonresonant pathways in the two-color two-photon processes.

DOI: 10.1103/PhysRevA.89.013415 PACS number(s): 32.80.Fb, 32.80.Hd

I. INTRODUCTION

The advent of new femtosecond pulse sources in the extreme ultraviolet (EUV) and soft-x-ray spectral range based on high-harmonic generation (HHG) and free-electron lasers (FELs) has given new impetus to investigations of nonlinear processes at high photon energies. Among others, the simplest nonlinear process, two-photon single ionization of atoms, attracts ever increasing attention [1–13]. In two-photon ionization (TPI) at photon energies typical of HHG and EUV-FEL sources, the first photon can excite an atom to high Rydberg states or ionize it. Then the second photon either ionizes the Rydberg atom or adds energy to the photoelectron giving rise to so-called above-threshold ionization (ATI) [14,15]. There are two types of TPI experiments: single-color [1–4] and two-color [5–13]. In the latter case the atom is ionized typically by a combination of EUV and infrared (IR) laser pulses. This type of experiment is especially attractive for studying near-threshold ionization where the emitted electron has low energy and its complicated dynamics is determined by the interaction with both radiation fields and with the ionic core.

In photoelectron spectroscopy [16] detailed information about the underlying processes can be obtained not only from the spectrum but also from photoelectron angular distributions (PADs), which are a sensitive test of theory. Recently, theoretical works [17,18] showed that the PAD in two-photon single ionization is very sensitive to the relative contribution of resonant and nonresonant ionization paths. They explicitly considered the single-color TPI of H and He atoms, where there are two outgoing channels, determined by s and d partial waves. In this case, the PAD crucially depends on the s and d amplitude ratio and on the phase-shift difference of the s and d waves. In particular, if either the resonant or the nonresonant ionization dominates, the phase-shift difference is equal to the scattering phase-shift difference at the energy of the outgoing electron, an intrinsic property of the atom. Conversely, if both resonant and nonresonant paths contribute, the phase-shift difference is no longer equal to the scattering phase-shift difference and depends on the pulse parameters such as pulse width. This prediction was very recently confirmed experimentally in single-color TPI of He by ultrashort EUV pulses [4]. It was demonstrated that the experimental s-d phase-shift difference sharply increases with excitation energy due to the contribution of the nonresonant path, in full agreement with theory. The additional phase associated with the simultaneous presence of both contributions is large when a Rydberg manifold is excited, and this phase and the amplitude ratio remain almost constant in the near-threshold region when the excitation energy increases through the threshold to the continuum [17,18].

Similar interplay between the resonant and nonresonant mechanisms is also expected for two-color two-photon ionization or ATI. In fact, it was demonstrated in experiments by Haber *et al.* [12] on He that when the excitation energy

of the first EUV pulse is close to the energy of one of the Rydberg states the PAD coincides with that obtained in the two-step picture accounting for the resonance pathway only, and therefore the phase-shift difference is close to the scattering one. This was recently confirmed by measurements of PADs in He with synchrotron radiation combined with IR laser pulses [13]. In contrast to these findings with EUV photon energies below the threshold, the phase-shift difference which can be derived from the measured PADs for the two-color two-photon ATI with EUV photon energies above the threshold [9] is considerably larger than the scattering phase-shift difference, indicating a significant contribution of the nonresonant path.

II. PRINCIPLE

In this work we suggest another approach to explore the role of the resonant and nonresonant mechanisms in the PADs of two-color TPI with measurements in the time domain, and we compare overlapping and nonoverlapping pulses. To illustrate the main idea it is instructive to consider the problem within the second-order time-dependent perturbation theory. Generalizing the expression for the amplitude of the two-photon transition presented in Ref. [19] to include multiple intermediate states, one can obtain the following expression for the amplitude of ionization (atomic units are used throughout unless otherwise indicated):

$$c_f = i\sum_\alpha \mu_{f\alpha}\mu_{\alpha i}\left[i\pi\hat{E}(\omega_{\alpha i})\hat{E}(\omega_{f\alpha}) + \mathrm{P}\int_{-\infty}^{\infty}\frac{\hat{E}(\omega)\hat{E}(\omega_{fi}-\omega)}{\omega_{\alpha i}-\omega}d\omega\right], \quad (1)$$

where $\mu_{\alpha i}$ and $\mu_{f\alpha}$ denote the dipole transition-matrix elements between initial i, intermediate α, and final f states; ω_i,ω_α, and ω_f are the corresponding eigenenergies; $\omega_{\alpha i} = \omega_\alpha - \omega_i$ etc.; P is the Cauchy principal value; and $\hat{E}(\omega)$ is the Fourier transform of the electric field $E(t)$. In principle, the sum should be taken over all the bound and continuum intermediate states α. The first and second terms of Eq. (1) are usually interpreted as a contribution of the resonant (or two-step) and nonresonant processes, respectively. In the case of ionization by EUV and IR pulses acting on the atom with some time delay, the Fourier transform of the field may be represented as

$$\hat{E}(\omega) = \hat{E}_X(\omega) + \hat{E}_{\mathrm{IR}}(\omega)e^{i\omega\tau}, \quad (2)$$

where the first and second terms correspond to the EUV and IR pulses, respectively, and τ denotes the delay between the pulses. In this case, taking into account that the IR frequency is much less than the typical excitation energy, Eq. (1) can be approximated by

$$c_f \approx i\sum_\alpha \mu_{f\alpha}\mu_{\alpha i}\left[i\pi\hat{E}_X(\omega_{\alpha i})\hat{E}_{\mathrm{IR}}(\omega_{f\alpha})e^{i\omega_{f\alpha}\tau} + \mathrm{P}\int_{-\infty}^{\infty}\hat{E}_X(\omega_{fi}-\omega)\hat{E}_{\mathrm{IR}}(\omega)e^{i\omega\tau}\times\left(\frac{1}{\omega_{\alpha i}-\omega}-\frac{1}{\omega_{f\alpha}-\omega}\right)d\omega\right]. \quad (3)$$

When the two pulses overlap ($\tau = 0$), both the first (resonant) and second (nonresonant) terms contribute to c_f, leading to a PAD different from the one expected for a pure resonant case with the scattering phase-shift difference. With increasing delay, the factors $e^{i\omega_{f\alpha}\tau}$ and $e^{i\omega\tau}$ start to oscillate, and the PAD changes with τ. One can show that at large $|\tau|$ (nonoverlapping pulses) Eq. (3) can be rewritten as

$$c_f \approx -\sum_\alpha \mu_{f\alpha}\mu_{\alpha i}\{1+\mathrm{sgn}(\tau)\}\pi\hat{E}_X(\omega_{\alpha i})\hat{E}_{\mathrm{IR}}(\omega_{f\alpha})e^{i\omega_{f\alpha}\tau}. \quad (4)$$

If $\tau < 0$ (the IR pulse comes first), then $\mathrm{sgn}(\tau) = -1$ and thus $c_f = 0$ (no TPI if the IR pulse comes before EUV). If $\tau > 0$ (the EUV pulse comes first), the long-lived Rydberg states will be ionized by the delayed IR pulse, but the PAD will have exactly the same shape as is expected for the resonant (two-step) process. The nonresonant part tends to zero since the probability to have two photons interacting with the atom simultaneously is negligibly small. Naturally, and as can be demonstrated using Eq. (4), the ATI also vanishes in this case since the electron wave packet produced by the EUV pulse leaves the interaction region before the IR pulse arrives.

Our computations based on solving the time-dependent Schrödinger equation (TDSE) for Ne ionization have shown that indeed the PADs strongly depend on the time delay between the pulses. In particular, the computations have revealed a qualitative difference in PADs for two extreme cases of completely overlapping and nonoverlapping pulses. This has allowed us to sort the experimental PADs, obtained under conditions where the time jitter of the pulses is large, and to separate the events with overlapping and nonoverlapping pulses. The results obtained agree with the theoretical predictions. This confirms the idea that it is possible to study experimentally the contribution of resonant and nonresonant path by measuring the PADs in TPI.

III. EXPERIMENT

The experiments were performed using the SCSS Test Accelerator [21,22] at SPring-8, which delivered 30-fs [1] linearly polarized EUV pulses at 30-Hz repetition rate. The coherence time of the pulses was 8 fs [1]. The EUV pulses were transported by two plane mirrors into a beam line and focused with a pair of elliptical and cylindrical mirrors into the interaction region to about 15 μm [full width at half maximum (FWHM)] in diameter. The photon energies of the EUV pulses were set to 21.3 and 24.3 eV, respectively, just below and above the ionization energy of neon atoms. IR 800-nm pulses were generated by a Ti:sapphire laser and electronically synchronized to the EUV pulses. The duration of the IR pulses was 30 fs [22]. The IR pulses intersected the EUV pulses at an angle of $\sim 1^\circ$. Their linear polarization direction nearly coincides with that of the EUV pulses. The effective intensity of the IR pulses was estimated to be 0.6×10^{12} W/cm^2 from the relative intensity of the first and second ATI peaks in He measured under the same conditions [23]. The temporal jitter between the EUV and IR pulses for a short measurement of a few minutes was ~ 0.5 ps [22,23]. The photoelectrons emitted due to simultaneous action of

EUV and IR pulses were accelerated through a velocity map imaging (VMI) spectrometer perpendicularly to both the propagation direction and linear polarization axis of the EUV and IR pulses, toward a position sensitive microchannel plate detector followed by a phosphor screen. The positions of the detected electrons were recorded using a gated CCD camera synchronized with the arrival time of the EUV pulses. The photoelectrons were recorded in series of 10^4 FEL shots each. The three-dimensional photoelectron momentum distribution was retrieved from the measured two-dimensional projection of the momentum distribution using a mathematical procedure based on Abel inversion [24], where we express the PAD in terms of a Legendre polynomial expansion. In TPI the PAD is expected to have the form $a[1 + \beta_2 P_2(\cos\theta) + \beta_4 P_4(\cos\theta)]$, where $P_n(x)$ is a Legendre polynomial, β_2 and β_4 are asymmetry parameters, and θ is the emission angle relative to the polarization axis. In single-photon ionization $\beta_4 \equiv 0$. To test the quantitative accuracy of the VMI setup and analysis, we analyzed the angular distribution of photoelectrons emitted from Ne by 24.3-eV FEL radiation only. The resulting value of $\beta_2 = -0.32 \pm 0.06$ is in very good agreement with the early experimental synchrotron radiation data -0.30 ± 0.08 [25] and -0.33 ± 0.06 [26].

IV. MODELING

For interpretation of the experimental results we solved numerically the TDSE in the single active electron approximation. Solving the TDSE is especially convenient for our task since it permits one to treat in a unified way the ionization of the Rydberg wave packet as well as the above-threshold ionization in the continuum. The details of the application of the TDSE to the problem of atom ionization in the combined field of the EUV and the IR pulses are given in earlier publications [27,28]. In order to make calculations feasible, we considered shorter EUV pulses than in the experiment, namely, with FWHM = 7 fs, which is close to the coherence time of the FEL pulses. However, we checked that the final result is only weakly sensitive to this duration. The atomic potential and the bound-state wave functions have been calculated in the Hartree-Slater (HS) approximation [29]. The local HS potential makes the TDSE calculations feasible. However, the accuracy of the PADs calculated with this potential is only about 20–30%. In particular, for the EUV photon energy 24.3 eV without the IR field (peak energy 2.7 eV) the calculations give $\beta_2 = -0.22$.

V. RESULTS AND DISCUSSION

For FEL photon energy 24.3 eV (the above-threshold case) when both EUV and IR pulses are present, the measured photoelectron spectrum integrated over emission angles is shown in Fig. 1(a). Beside the main photoline at 2.7 eV, two sidebands are clearly seen. Here, we set the time delay to zero. Note that due to the temporal jitter of 0.5 ps between the EUV and IR pulses the two pulses with pulse widths of 30 fs temporally overlap occasionally. However, the appearance of the sidebands clearly indicates that in the selected measurements the EUV and IR pulses overlapped. Figures 1(b) and 1(c) show (dashed lines) the corresponding angular distributions of photoelectrons at the low-energy sideband (LSB) and high-energy sideband (HSB), respectively. The solid lines show the results of TDSE calculations. The fitted asymmetry parameters β_2 and β_4 are shown in Table I. The agreement between the measured and calculated values is rather good. We note that calculations have been done for a complete overlap of the EUV and IR pulses with intensity 0.6×10^{12} W/cm^2, which is equal to the effective intensity of the IR pulses in the experiment.

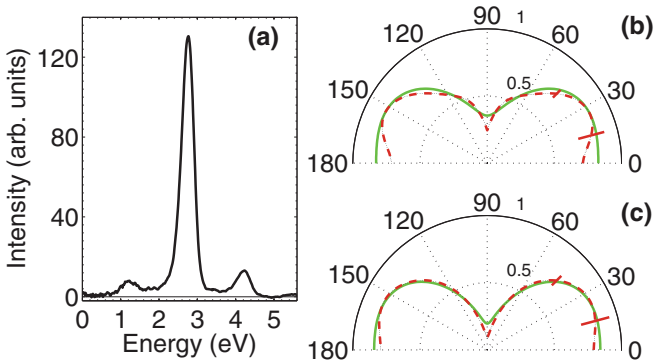

FIG. 1. (Color online) (a) Spectrum of photoelectrons measured at the EUV photon energy of 24.3 eV. The central peak at 2.7 eV is due to ionization of the Ne $2p$ subshell by the EUV pulse. Two smaller peaks at the energies of 1.15 and 4.25 eV are sidebands which arise due to interaction with the IR field. Right panels show the measured (dashed lines) and calculated (solid lines) angular distributions of photoelectrons at the LSB (b) and the HSB (c). The bars at 15 and 45° show typical error bars of the measured angular distributions.

Next consider the case of FEL photon energy 21.3 eV (the below-threshold case). Here two experiments in different conditions were done. In experiment 1, the IR pulse was delayed by 10 ps after the EUV pulse. In experiment 2, the delay of the IR pulses was electronically set to 0 ps. However, due to jitter of 0.5 ps of the EUV pulses, the temporal overlap between the pulses occurred rarely. Figure 2(a) depicts the photoelectron spectrum integrated over emission angles measured in experiment 1. With an EUV pulse spectral width of 0.2 eV, a wave packet of Rydberg states with $n = 7$–11 is excited [20]. Since the lifetime of Rydberg states is of the

TABLE I. Experimental and theoretical values of asymmetry parameters β_2 and β_4 for EUV photon energies E_γ and different photoelectron energies E_e. The third line denoted (a) corresponds to nonoverlapping pulses with 10-ps delay (experiment 1). The fourth line denoted (b) corresponds to overlapping pulses (0-ps delay). The fifth line denoted(c) corresponds to nonoverlapping pulses from experiment 2. The theoretical parameters are averaged over the Rydberg states occurring within the bandwidth of the FEL.

		Experiment		Calculation	
E_γ (eV)	E_e (eV)	β_2	β_4	β_2	β_4
24.3	1.15	0.65 ± 0.09	-0.41 ± 0.11	0.63	−0.27
	4.25	1.13 ± 0.06	-0.51 ± 0.24	0.98	−0.35
21.3	1.25(a)	1.14 ± 0.11	0.28 ± 0.17	0.96	0.62
	1.25(b)	0.66 ± 0.33	-0.52 ± 0.23	0.54	−0.61
	1.25(c)	0.99 ± 0.16	0.26 ± 0.23	0.96	0.62

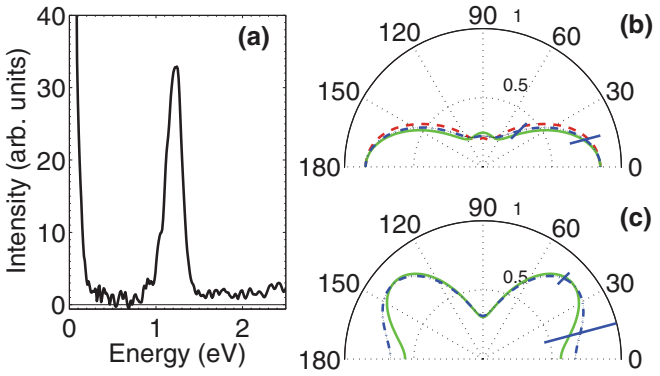

FIG. 2. (Color online) (a) Spectrum of photoelectrons measured at photon energy 21.3 eV. The peak at 1.25 eV corresponds to the ionization of the Rydberg wave packet by the IR field. (b) The angular distribution of photoelectrons of the 1.25-eV peak for the case when EUV and IR pulses are not overlapped. Dashed line, measured in experiment 1 (10-ps delay); dash-dotted line, measured in experiment 2 (0-ps delay) by selecting the nonoverlapping events; solid line, calculations. (c) The angular distribution of photoelectrons of the 1.25-eV peak for the case in which EUV and IR pulses are overlapped. Dash-dotted, measured in experiment 2 (0-ps delay) with selection of the overlapping events; solid line, calculations. The bars at 15 and 45° show typical error bars of the measured angular distributions.

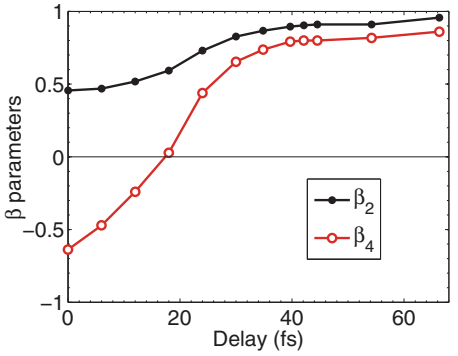

FIG. 3. (Color online) The calculated dependence of asymmetry parameters β_2 (closed circle) and β_4 (open circle) on delay between EUV and IR pulses for the case of EUV photon energy 21.3 eV. The parameters are shown for the angular distributions at the maximum of the peak (1.25 eV).

order of microseconds, the radiative decay practically does not influence the Rydberg wave packet, which develops in the ionic potential before being ionized by the IR pulse. The following IR ionization of the Rydberg states leads to appearance of the photoelectron peak at the energy of 1.25 eV as seen in the figure. The increase of the electron yield at zero energy is due to single-photon ionization by the high-energy tail of the EUV spectrum. The angular distribution of 1.25-eV photoelectrons is shown in Fig. 2(b) (dashed line) together with the theoretical results (solid line), and the corresponding β parameters are given in Table I (third line). The general agreement between theory and experiment is reasonable.

Consider now the case of FEL photon energy 21.3 eV with the IR pulses overlapped with the EUV pulses. The calculated PAD is shown in Fig. 2(c) (solid line). Comparing it with the calculated PAD for the nonoverlapping case in Fig. 2(b), one clearly sees that theory predicts strong dependence of the PADs on the overlap of the EUV and IR pulses. In order to see it in more detail we have calculated the PAD as a function of pulse delay τ. Figure 3 shows the results of calculations. Both parameters β_2 and β_4 change with delay. Especially, β_4, which appears only in the presence of the dressing IR field, varies considerably and even changes its sign. To measure the dependence of the PADs on the overlap of the EUV and IR pulses in the present experiment, we extracted the overlapping and nonoverlapping contributions from the measured data of experiment 2 by applying a Bayesian approach [30] to the analysis.

The number of counts in a single image was not sufficient to perform shot by shot inversion and fitting, so to distinguish the overlapping from nonoverlapping pulses for the case of FEL photon energy 21.3 eV (the below-threshold case) we employed the following procedure. We assume that there are two types of PAD, characteristic of overlapping or nonoverlapping pulses, and all images are of one type or the other, or are a linear sum of these two types. Furthermore, we hypothesize that the calculated distributions are a reasonable first approximation to these two types of PAD, but we do not require them to be rigorously correct.

Each image (shot) was symmetrized along the two axes parallel and perpendicular to the electric vector, and then the intensities $I(A)$ and $I(B)$ were integrated over the areas A, $\phi = 0$ to 15°, and B, $\phi = 30$ to 60°. Here ϕ is the angle between the direction of the light polarization and the direction of the electron emission projected onto the imaging plane. The images were then sorted into two groups: group I for events satisfying $I(A) > I(B)$ and group II for events satisfying $I(A) < I(B)$. This criterion is based on the theoretical PADs in Figs. 2(b) and 2(c), which predict that the events of group I correspond to primarily nonoverlapping events while those of group II correspond to primarily overlapping events. This provides us with a first estimate of the experimental PADs of the two cases.

Even though the criterion of different integral intensities is a rather weak assumption, it is possible that the data may be biased by noise using this procedure. To test for this we performed further analysis. In one test, the data were symmetrized about one axis only, such as the polarization axis. The selection criterion was then applied to one half of the image, but only the other half of the image was considered in the analysis. This gave results consistent with the previous analysis, using the whole image, with a higher estimated error. Clearly bias due to noise in one half of the image should not cause bias in the other half. Similarly, three of the four quadrants were used for selection, and only the fourth was used to generate the final PAD; alternatively, one was used for selection and the other three quadrants were used to generate the image. This again gave consistent PADs; we therefore conclude that the initial hypotheses are justified *a posteriori*.

For the nonoverlapping case, the experimental PAD is compared with the theoretical PAD in Fig. 2(b). In Fig. 2(c), the experimental PAD is compared with the theoretical PAD for the overlapping case. The resulting β_2 and β_4 values for the overlapping and nonoverlapping cases are also listed in

Table I. The general agreement between experiment and theory confirms that the PAD strongly depends on the overlap of the EUV and IR pulses. The observed dependence of the PADs on the pulse overlap stems from a variation of relative contributions of resonant and nonresonant paths of ionization which leads to the variation of the amplitude ratio and the additional phase-shift difference (between p and f final electron waves in the Ne case) beyond the scattering phase-shift difference [17,18]. The PAD for the high-energy sideband in Fig. 1(c) is similar to the PAD for the overlapping case in Fig. 2(c). This similarity may be understood by the fact that the PAD changes continuously across the ionization threshold [17,18].

We note that studies of the the PADs in two-color TPI and their dependence on the time delay between the pulses were previously reported [7,10,12]. However, in Ref. [7], the time-delay dependence was studied on the attosecond scale and is connected with the relative phase of the EUV and IR pulses, which is not fixed in our experiment. On the other hand, in Refs. [10,12] no time-delay dependence of the PADs on the femtosecond scale was detected within experimental error for He atoms excited both below and above threshold. According to our TDSE simulations, the He atom indeed represents a special case in which the PAD barely varies with delay, accidentally, for the particular combination of photon energies used. The details are presented elsewhere [23].

VI. CONCLUSIONS

In conclusion, we have investigated experimentally and theoretically the PADs for EUV + IR TPI of Ne atoms, with EUV excitation to both below and above the ionization threshold. We have shown theoretically that the PADs strongly depend on the time delay between the EUV and IR pulses and confirmed this experimentally for two extreme cases of complete overlapping and nonoverlapping pulses. This dependence is associated with the different contributions of the resonant and nonresonant pathways of ionization. Therefore, investigations of the time-delay dependence of the PADs in TPI make it possible to study the fundamental problem of the relative importance of resonant and nonresonant processes in photoionization. Our work is a first step in this direction which will have impact on the broad area of atomic and molecular physics as well as surface and condensed-matter physics.

ACKNOWLEDGMENTS

We are grateful to the SPring-8 Compact Self-Amplified Spontaneous Emission Source Test Accelerator Operation Group at RIKEN for continuous support in the course of the studies and to the staff of the technical service section in Institute of Multidisciplinary Research for Advanced Materials (IMRAM), Tohoku University, for their assistance in constructing the apparatus. This study was supported by the X-Ray Free Electron Laser (XFEL) Utilization Research Project and the XFEL Priority Strategy Program of Ministry of Education, Culture, Sports, Science, and Technology of Japan (MEXT); by the Management Expenses Grants for National Universities Corporations from MEXT; by Grants-in-Aid for Scientific Research from Japan Society for the Promotion of Science (JSPS) (Grants No. 21244062 and No. 22740264); and by the IMRAM research program. SM would like to thank JSPS for financial support. NMK acknowledges the hospitality and financial support of IMRAM, Tohoku University. KLI gratefully acknowledges support by the APSA Project (Japan), KAKENHI (Grants No. 23656043 and No. 25286064), and the Cooperative Research Program of "Network Joint Research Center for Materials and Devices" (Japan).

[1] R. Moshammer *et al.*, Opt. Express **19**, 21698 (2011).
[2] M. Meyer *et al.*, Phys. Rev. Lett. **104**, 213001 (2010).
[3] T. Sato *et al.*, J. Phys. B **44**, 161001 (2011).
[4] R. Ma *et al.*, J. Phys. B **46**, 164018 (2013).
[5] O. Guyetand *et al.*, J. Phys. B **38**, L357 (2005).
[6] M. Meyer *et al.*, Phys. Rev. A **74**, 011401 (2006).
[7] O. Guyetand *et al.*, J. Phys. B **41**, 051002 (2008).
[8] M. Meyer *et al.*, Phys. Rev. Lett. **101**, 193002 (2008).
[9] L. H. Haber, B. Doughty, and S. R. Leone, Phys. Rev. A **84**, 013416 (2011).
[10] L. H. Haber, B. Doughty, and S. R. Leone, Mol. Phys. **108**, 1241 (2010).
[11] L. H. Haber, B. Doughty, and S. R. Leone, J. Phys. Chem. A **113**, 13152 (2009).
[12] L. H. Haber, B. Doughty, and S. R. Leone, Phys. Rev. A **79**, 031401(R) (2009).
[13] P. O'Keeffe, A. Mihelic, P. Bolognesi, M. Zitnik, A. Moise, R. Richter, and L. Avaldi, New J. Phys. **15**, 013023 (2013).
[14] T. Brabec and F. Krausz, Rev. Mod. Phys. **72**, 545 (2000).
[15] P. Agostini and L. F. DiMauro, Rep. Prog. Phys. **67**, 813 (2004).
[16] *VUV and Soft X-Ray Photoionization*, edited by U. Becker and D. A. Shirley (Plenum, New York, 1996).
[17] K. L. Ishikawa and K. Ueda, Phys. Rev. Lett. **108**, 033003 (2012).
[18] K. L. Ishikawa and K. Ueda, Applied Sciences **3**, 189 (2013).
[19] N. Dudovich, B. Dayan, S. M. Gallagher Faeder, and Y. Silberberg, Phys. Rev. Lett. **86**, 47 (2001).
[20] A. Kramida, Yu. Ralchenko, J. Reader, and NIST ASD Team 2012, NIST Atomic Spectra Database (version 5.0), http://physics.nist.gov/asd.
[21] T. Shintake *et al.*, Nat. Photon. **2**, 555 (2008).
[22] M. Yabashi *et al.*, J. Phys. B **46**, 164001 (2013).
[23] S. Mondal *et al.*, J. Phys. B **46**, 205601 (2013).
[24] M. J. J. Vrakking, Rev. Sci. Instrum. **72**, 4084 (2001).

[25] K. Codling, R. G. Houlgate, J. B. West, and P. R. Woodruff, J. Phys. B **9**, L83 (1976).

[26] S. H. Southworth, A. C. Parr, J. E. Hardis, J. L. Dehmer, and D. M. P. Holland, Nucl. Instrum. Methods Phys. Res. A **246**, 782 (1986).

[27] A. K. Kazansky and N. M. Kabachnik, J. Phys. B **40**, 2163 (2007).

[28] A. K. Kazansky and N. M. Kabachnik, J. Phys. B **40**, 3413 (2007).

[29] F. Herman and S. Skillman, *Atomic Structure Calculations* (Prentice-Hall, Englewood Cliffs, NJ, 1963).

[30] D. Sivia, *Data Analysis—A Bayesian Tutorial* (Oxford University, Oxford, 2006).